Platinum Nanoparticles

International Edition: DOI: 10.1002/anie.201508985
German Edition: DOI: 10.1002/ange.201508985

Nanoparticle-Mediated Intervalence Charge Transfer: Core-Size Effects

*Peiguang Hu, Limei Chen, Christopher P. Deming, Xiongwu Kang, and Shaowei Chen**

Abstract: *Two types of platinum nanoparticles (NPs) functionalized with ethynylferrocene were prepared. The subnanometer-sized NPs (Pt_{10}eFc) showed semiconductor-like characteristics with a bandgap of about 1.0 eV, and the other was metal-like with a core size of about 2 nm (Pt_{314}eFc) and no significant bandgap. IR spectroscopic measurements showed a clear red-shift of the C≡C and ferrocenyl ring =C−H vibrational energies with increasing particle core size owing to enhanced intraparticle charge delocalization between the particle-bound ferrocenyl moieties. Electrochemical measurements showed two pairs of voltammetric peaks owing to intervalence charge transfer between the ferrocenyl groups on the nanoparticle surface, which was apparently weaker with Pt_{10}eFc than with Pt_{314}eFc. Significantly, the former might be markedly enhanced with UV photoirradiation owing to enhanced nanoparticle electronic conductivity, whereas no apparent effects were observed with the latter.*

In recent years, it has been found that electronic communication may occur between nanoparticle-bound functional moieties when they are bonded to the nanoparticle surface by conjugated metal–ligand interfacial linkages.[1] This leads to the emergence of new optical and electronic properties that are analogous to those of their dimeric derivatives. For instance, when ferrocenyl moieties are bound to ruthenium nanoparticle surfaces by ruthenium–carbene (Ru=C) π bonds, electrochemical measurements exhibit two pairs of voltammetric peaks consistent with the well-known intervalence charge transfer (IVCT) of biferrocene derivatives bridged with conjugated chemical linkers.[2] Such nanoparticle-mediated intraparticle charge delocalization has also been observed with other functional moieties, and facilitated by the conducting metal cores. For instance, electron injection into the metal cores by chemical reduction is found to readily enhance intraparticle charge delocalization, whereas opposite effects are observed by chemical oxidation.[3] In these earlier studies, the nanoparticle metal cores are typically over 2 nm in diameter, and hence exhibit electronic conductivity analogous to that of the corresponding bulk metal.[4]

However, when the core size of the metal nanoparticles diminishes to the subnanometer regime, comparable to the Fermi wavelength of an electron, the nanoparticles become molecule-like, with the emergence of a nonzero HOMO–LUMO bandgap, akin to semiconductor materials.[4] Such metal nanoclusters, consisting of several to a few tens of atoms, show extraordinary high specific surface area, significantly modified optical properties, and discrete energy levels.[5] Thus, an immediate question arises. When functional moieties are bonded to subnanometer-sized particle surfaces, will effective electronic communication still occur between them? This is the primary motivation of the present work.

Herein, we compare the IVCT behaviors of two ferrocene-functionalized Pt nanoparticles, one with a core size about 2 nm (metal-like) and the other in the subnanometer regime (semiconductor-like). The ferrocenyl moieties were incorporated onto the nanoparticle surface by ligand-exchange reactions of triphenylphosphine (PPh_3)-stabilized platinum nanoparticles with ethynylferrocene (eFc) by taking advantage of the strong affinity of acetylene (C≡C) group to transition-metal surfaces forming metal–vinylidene (M=C=CH) or acetylide (M−C≡) interfacial bonds (for details, see the Experimental Section).[3,6] The structure of the subnanometer-sized PteFc clusters was first examined with MALDI-TOF mass spectrometric measurements. From the mass spectrum in Figure 1, a broad peak is observed centered around 2000 Da, suggesting that on average the nanoclusters consist of a Pt_{10} core, and the spikes at 1371, 1498, 1887, and 2092 Da indicates that along with Pt_{10} clusters, Pt_7 is another

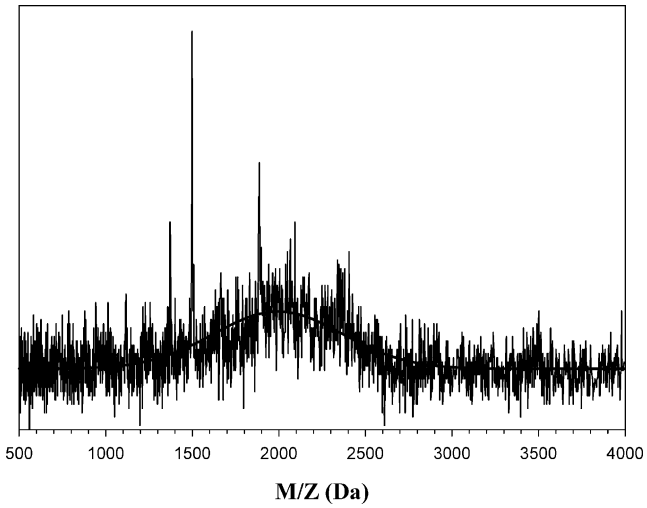

Figure 1. MALDI-TOF mass spectrum of Pt_{10}eFc nanoclusters. Noisy curve: experimental data; smooth curve: Gaussian fit.

[*] P. Hu, L. Chen, C. P. Deming, Prof. Dr. X. Kang,[+] Prof. Dr. S. Chen
Department of Chemistry and Biochemistry, University of California
1156 High Street, Santa Cruz, CA 95064 (USA)
E-mail: shaowei@ucsc.edu

[+] Present address: New Energy Research Center, School of Environment and Energy, South China University of Technology
Guangzhou Higher Education Mega Centre, Guangzhou 510006 (China)

Supporting information for this article is available on the WWW under http://dx.doi.org/10.1002/anie.201508985.

major population in the sample. This corresponds to a core size of less than 1 nm for the Pt clusters.[7] Note that whereas conventional TEM is not a reliable method for evaluating nanoparticles in the subnanometer size range,[8] the Pt nanoparticles prepared by thermolysis of $PtCl_2$ in 1,2-propanediol are much larger and can be readily characterized by TEM measurements. A representative TEM image of the nanoparticles is given in the Supporting Information, Figure S1. It can be clearly seen that the nanoparticles were dispersed very well without apparent aggregation, indicating effective protection of the nanoparticles by the capping ligands. Furthermore, the Pt nanoparticle core size was estimated to be 2.08 ± 0.37 nm, as manifested by the core size histogram (Supporting Information, Figure S1 inset), based on a statistical analysis of more than 100 nanoparticles. Assuming a truncated octahedral structure, the metal core of the nanoparticles was estimated to consist of about 314 Pt atoms.[9] Therefore, these two nanoparticles were referred to as Pt_{10}eFc and Pt_{314}eFc, respectively.

It is well-known that when the size of metal nanoparticles diminishes to the subnanometer regime, a non-zero HOMO–LUMO bandgap starts to emerge, as manifested in optical and electrochemical measurements.[4,10] Figure 2A depicts the UV/Vis absorption spectra of the Pt_{10}eFc and Pt_{314}eFc nanoparticles. It can be seen that both nanoparticles exhibited a broad absorption band centered at around 3.36 eV (368 nm), arising from the d–d transitions of the ferrocenyl moieties;[11] and for the Pt_{10}eFc sample, two additional absorption peaks can be identified around 2.62 eV (473 nm) and 1.75 eV (708 nm), which may be ascribed to interband transitions of the subnanometer-sized Pt_{10} clusters.[12] In fact, by extrapolating the absorption profiles to the *x*-axis (dashed curves), the bandgap of the Pt_{10}eFc nanoparticles can be estimated to be 1.0 eV whereas the larger Pt_{314}eFc nanoparticles shows an intercept of only 0.4 eV.

The incorporation of ferrocenyl moieties onto the nanoparticle surface was confirmed and quantified by ^{1}H NMR measurements. Figure 2B shows the ^{1}H NMR spectra of the Pt_{10}eFc and the Pt_{314}eFc nanoparticles. It can be seen that both spectra exhibit two broad peaks centered around 7.45 and 4.25 ppm. The former may be assigned to the phenyl protons of PPh_3, and the latter to the ferrocenyl protons of eFc, suggesting incomplete replacement of the original PPh_3 ligands by eFc. Furthermore, no alkynyl (≡C–H) protons at 2.71 ppm can be seen in both samples, indicating that both nanoparticles are spectroscopically clean and free of excess free eFc ligands. Furthermore, based on the integrated peak areas of the phenyl and ferrocenyl ring protons, the molar ratio of the eFc and PPh_3 ligands on the nanoparticle surface was estimated to be 4.44:1 for Pt_{10}eFc and 1.14:1 for Pt_{314}eFc.

The successful incorporation of the ferrocenyl ligands onto the nanoparticle surface was also manifested in FTIR measurements. From Figure 3, it can be seen that whereas PPh_3 monomers displayed multiple overtones/combination peaks within the range of 1600 to 2000 cm^{-1}, the features diminished markedly with the two nanoparticle samples (along with the phenyl ring =C–H vibration at 3066 cm^{-1}), suggesting a decrease of the PPh_3 concentration. Furthermore, for the eFc monomers, the terminal ≡C–H vibration can be clearly identified at 3292 cm^{-1}, the C≡C stretch at 2109 cm^{-1}, and the ferrocenyl ring =C–H stretch at 3113 cm^{-1}.

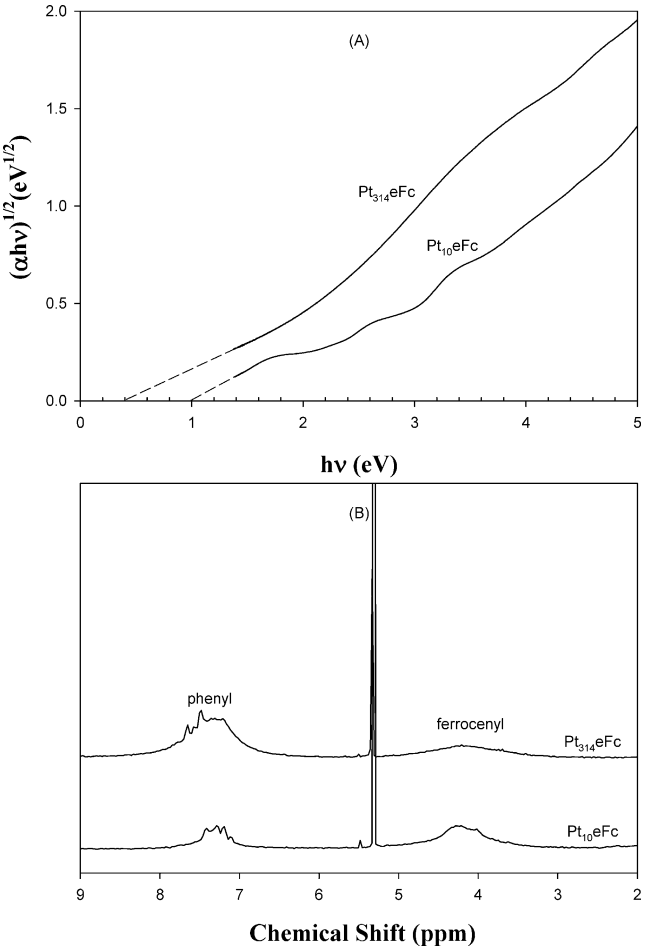

Figure 2. A) UV/Vis absorption spectra of the Pt_{10}eFc and Pt_{314}eFc nanoparticles in CH_2Cl_2. α is the optical absorbance and $h\nu$ is the photon energy. Dashed lines are linear extrapolation to the *x*-axis. B) ^{1}H NMR spectra of the Pt_{10}eFc and Pt_{314}eFc nanoparticles in CD_2Cl_2.

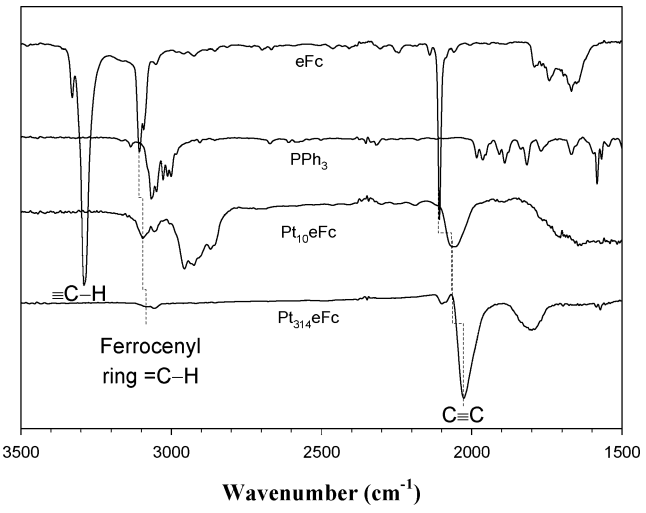

Figure 3. FTIR spectra of Pt_{10}eFc, Pt_{314}eFc nanoparticles, and monomeric eFc and PPh_3 ligands.

Yet when the ligands were bound onto Pt nanoparticle surface by ligand-exchange reactions, the sharp peak at 3291 cm^{-1} vanished for both the Pt_{10}eFc and Pt_{314}eFc nanoparticles, indicating ready cleavage of the ≡C–H bond and the formation of Pt–C≡ or Pt=C=CH– bonds at the metal–ligand interface (this also shows that both nanoparticle samples were indeed free of monomeric eFc).[6b] Furthermore, the ferrocenyl ring =C–H stretch and the C≡C stretch both exhibited a marked red-shift to 3095 and 2060 cm^{-1} for Pt_{10}eFc, and 3092 and 2024 cm^{-1} for Pt_{314}eFc, respectively. This may be ascribed to intraparticle charge delocalization between the particle-bound ferrocene moieties as a result of the conjugated metal-ligand interfacial bonds, as observed previously.[6b,13] Furthermore, the fact that the =C–H and C≡C stretches were at lower energy with the larger Pt_{314}eFc nanoparticles than with the smaller Pt_{10}eFc suggests better conjugation between the ferrocenyl moieties in Pt_{314}eFc than in Pt_{10}eFc, most probably because of the nonzero bandgap of the subnanometer-sized metal cores that diminished the electronic conductivity of the nanoclusters, as compared to the large nanoparticles that are anticipated to behave analogously to bulk metal.[4]

Interestingly, the apparent difference of the electronic structure of the nanoparticle metal cores led to marked discrepancy of the nanoparticle electrochemical behaviors. Figure 4 depicts the square-wave voltammograms (SWVs) of A) Pt_{314}eFc and B) Pt_{10}eFc nanoparticles in the dark and under UV photoirradiation (254 nm, 4.89 eV) with 0.1 M TBAP in CH_2Cl_2. From (A), two pairs of voltammetric peaks (dotted curves) can be clearly seen in the dark at the formal potentials ($E^{o\prime}$) of +0.042 V and +0.32 V (vs. Fc^+/Fc), in contrast to the featureless profiles observed with TBAP alone (solid curves). These may be ascribed to the nanoparticle-mediated intervalence charge transfer of the particle-bound ferrocenyl moieties as a result of the conjugated metal-ligand interfacial bonds, and the peak spacing ($\Delta E^{o\prime}$) of 0.28 V indicates that the nanoparticles behaved analogously to a class II complex as defined by Robin and Day.[1c,14] Consistent results are observed when the solution was exposed to UV irradiation (dashed curves), where the two pairs of voltammetric peaks now appeared at +0.021 and +0.30 V with an identical $\Delta E^{o\prime}$ of 0.28 V. This may be accounted for by the lack of dependence of the nanoparticle electronic conductivity on photoirradiation because the metal cores are sufficiently big such that the nanoparticles behaved like the bulk metal.[4]

For the much smaller Pt_{10}eFc particles, markedly different voltammetric responses were seen, as manifested in (B). First, whereas there are also two pairs of voltammetric peaks within the potential range of −0.4 to +0.6 V when the voltammograms were acquired in the dark (dotted curves), the peaks can only be resolved by deconvolution at $E^{o\prime}$ = +0.042 and +0.22 V (vs Fc^+/Fc). The peak potential spacing of $\Delta E^{o\prime}$ = 0.18 V suggests that the Pt_{10}eFc nanoparticles fell into the intermediate between a class I and II complex.[1c,14] The fact that $\Delta E^{o\prime}$ is much smaller than that of Pt_{314}eFc signifies reduced intraparticle charge delocalization between the particle-bound ferrocenyl moieties, which is likely due to the ultrasmall particle core size and semiconductor-like

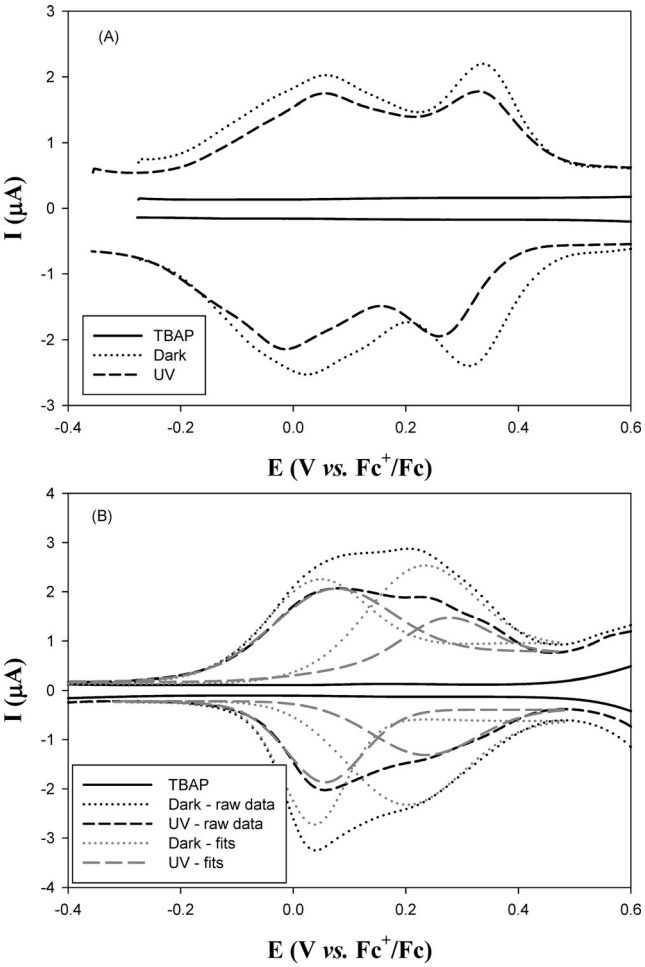

Figure 4. SWVs of A) Pt_{314}eFc and B) Pt_{10}eFc nanoparticles at a gold electrode in 0.1 M TBAP in CH_2Cl_2 in the dark and under UV irradiation. Electrode surface areas: Pt_{314}eFc 0.87 mm^2, Pt_{10}eFc 2.41 mm^2. Nanoparticle concentrations: Pt_{314}eFc 5 mg mL^{-1}, Pt_{10}eFc 2 mg mL^{-1}. Increment of potential 2 mV, amplitude 25 mV, frequency 15 Hz. In panel (B), black curves are experimental data and gray curves are deconvolution fits.

electronic conductivity, akin to the results where the structure of the chemical bridge was found to significantly impact the IVCT of biferrocene derivatives.[2c,15] Interestingly, upon the exposure to UV photoirradiation, the two pairs of voltammetric peaks now appeared at +0.060 and +0.26 V (dashed curves), and $\Delta E^{o\prime}$ increased by 20 mV to 0.20 V. This may be accounted for by the photo-enhanced nanoparticle electronic conductivity,[16] leading to improved intraparticle charge delocalization between the surface ferrocenyl moieties, in contrast to the results of the larger Pt_{314}eFc nanoparticles.

In summary, the results presented above indicate when the nanoparticle core size diminishes to the subnanometer regime such that an apparent bandgap emerges, IVCT between nanoparticle-bound functional moieties diminishes markedly, in contrast to large nanoparticles where the cores behave like the bulk metal, as manifested in spectroscopic and electrochemical measurements. Yet, because of the semiconductor-like electronic characteristics of the subnanometer-sized clusters, photoirradiation can be used as an effective

method to enhance the nanoparticle electronic conductivity and hence intraparticle charge delocalization, whereas no such effects are observed with the large counterparts. This further highlights the unique significance of metal core structures in the manipulation of nanoparticle charge-transfer dynamics.

Experimental Section

Chemicals: Platinum(II) chloride ($PtCl_2$, 73% Pt, ACROS), hydrochloric acid (HCl, 12 M, Fisher Scientific), tetra-*n*-octylammonium bromide (TOABr, 98%, Cole Parmer), triphenylphosphine (PPh_3, 99%+, ACROS), ethynylferrocene (eFc, 97%, ACROS), sodium acetate (NaOAc, MC&B), and sodium carbonate (Na_2CO_3, 99%, Fisher Scientific) were all used as received without any further purification. Solvents were purchased at the highest purity available from typical commercial sources and also used as received. Tetra-*n*-butylammonium perchlorate (TBAP, 98%, TCI America) was used after recrystallization 4 times in ethanol.

Synthesis of ethynylferrocene-functionalized platinum (PteFc) nanoparticles: Platinum nanoparticles of two different sizes were prepared. The synthetic procedure for subnanometer-sized Pt clusters was adopted from previous reports.[17] In a typical reaction, $PtCl_2$ (0.1 mmol) was dissolved in HCl (1 mL, 12.1 M) at 100 °C. The solution was then added to a toluene solution of TOABr (0.3 mmol in 30 mL) and stirred vigorously for 1 h. The organic phase was collected and magnetically stirred overnight after the addition of 0.3 mmol PPh_3, generating a white precipitate. The white precipitate was then collected by centrifugation and dispersed in an ethanol–water (30 mL:5 mL) mixture, into which CO was bubbled for 3 h. The solution was then under stirring for 12 h leading to the production of an orange precipitate. This signified the formation of subnanometer-sized Pt clusters. The orange precipitate was collected by centrifugation, rinsed three times with ethanol to remove water, and then washed five times with CH_2Cl_2 and isooctane (1:70) to remove excessive TOABr and PPh_3, affording purified PPh_3-stablized Pt ($PtPPh_3$) clusters. The nanoclusters were then mixed with eFc (0.3 mmol) in CH_2Cl_2 (1 mL) and stirred for 2 d, before the solution was dried by bubbling N_2 and washed with isooctane five times to remove monomeric ligands, leading to the preparation of ferrocene-functionalized Pt nanoclusters (Pt_{10}eFc).

To prepare larger Pt nanoparticles capped with eFc, a different procedure was used. First, PPh_3-protected platinum nanoparticles were synthesized by the self-assembly of PPh_3 onto the surface of "bare" Pt colloids that were synthesized by thermolytic reduction of $PtCl_2$ in 1,2-propanediol.[1c,18] Experimentally, $PtCl_2$ (0.1 mmol) was dissolved in HCl (3 mL, 12.1 M). The solution was then condensed to 1 mL, neutralized with sodium carbonate, and centrifuged to remove unsolved salts. The supernatant and NaOAc (1 mmol, 82 mg) were added to 1,2-propanediol (100 mL). The mixed solution was heated at 165 °C under vigorous stirring for 1 h. Toluene (50 mL) with PPh_3 (0.3 mmol; threefold molar excess of $PtCl_2$) was added after the solution was cooled down to room temperature, and the mixed solution was stirred magnetically for overnight. The toluene phase was then collected, dried by rotary evaporation, and rinsed extensively with excessive acetonitrile to obtain PPh_3-capped Pt nanoparticles. Exchange reactions with eFc were carried out in a similar fashion by adding a calculated amount of eFc into the $PtPPh_3$ nanoparticle solution in CH_2Cl_2 under magnetic stirring for 2 d, affording Pt_{314}eFc nanoparticles.

Characterization: The morphology and sizes of the PteFc nanoparticles were characterized by transmission electron microscopic (TEM) studies (Philips CM300 at 300 kV). UV/Vis spectra were collected with a UNICAM ATI UV4 spectrometer. FTIR measurements were carried out with a PerkinElmer FTIR spectrometer (Spectrum One, spectral resolution 4 cm^{-1}); the samples were prepared by casting the particle solutions onto a NaCl disk. ^1H NMR spectroscopic measurements were carried out by using concentrated nanoparticle solutions in CD_2Cl_2 with a Varian Unity 500 MHz NMR spectrometer. MALDI-TOF mass spectra were acquired by using an Ettan MALDI-TOF Pro (Amersham Biosciences) spectrometer equipped with a standard UV nitrogen laser (337 nm). The ions formed by the irradiation of laser were detected by a linear/reflectron time-of-flight mass spectrometer. The accelerating voltage was held at 20 kV and positive-ion mode was used. The platinum cluster solutions in CH_2Cl_2 was mixed with the DCTB matrix (10 mg mL^{-1} in CH_2Cl_2) and was then applied to the sample plate and air-dried. The laser beam was focused on a stainless steel plate where the samples were spotted.

Electrochemistry: Voltammetric measurements were carried out either in the dark or under UV photoirradiation (254 nm) with a CHI 440 electrochemical workstation. A polycrystalline gold disk electrode (sealed in glass tubing) was used as the working electrode. A Ag/AgCl wire and a Pt coil were used as the reference and counter electrodes, respectively. Note that experimentally the reference electrode was calibrated against the formal potential of the ferrocenium/ferrocene couple (Fc^+/Fc). The gold electrode was first polished with alumina slurries of 0.5 μm and then cleaned by sonication in 0.1 M HNO_3, H_2SO_4, and Nanopure water successively. Prior to data collection, the electrolyte solution was deaerated by bubbling ultra-high-purity N_2 for at least 20 min and blanketed with a nitrogen atmosphere during the entire experimental procedure.

Acknowledgements

This work was supported in part by the National Science Foundation (CHE-1265635 and DMR-1409396). TEM work was performed at the National Center for Electron Microscopy, Lawrence Berkeley National Laboratory, as part of a user project.

Keywords: band gaps · ferrocene · intervalence charge transfer · photoirradiation · platinum nanoparticles

How to cite: *Angew. Chem. Int. Ed.* **2016**, *55*, 1455–1459
Angew. Chem. **2016**, *128*, 1477–1481

[1] a) W. Chen, L. E. Brown, J. P. Konopelski, S. W. Chen, *Chem. Phys. Lett.* **2009**, *471*, 283–285; b) L. M. Chen, Y. Song, P. G. Hu, C. P. Deming, Y. Guo, S. W. Chen, *Phys. Chem. Chem. Phys.* **2014**, *16*, 18736–18742; c) W. Chen, S. W. Chen, F. Z. Ding, H. B. Wang, L. E. Brown, J. P. Konopelski, *J. Am. Chem. Soc.* **2008**, *130*, 12156–12162.

[2] a) G. Ferguson, C. Glidewell, G. Opromolla, C. M. Zakaria, P. Zanello, *J. Organomet. Chem.* **1996**, *517*, 183–190; b) T. Mochida, E. Nagabuchi, M. Takahashi, H. Mori, *Chem. Commun.* **2014**, *50*, 2481–2483; c) W. H. Morrison, S. Krogsrud, D. N. Hendrickson, *Inorg. Chem.* **1973**, *12*, 1998–2004.

[3] X. W. Kang, N. B. Zuckerman, J. P. Konopelski, S. W. Chen, *Angew. Chem. Int. Ed.* **2010**, *49*, 9496–9499; *Angew. Chem.* **2010**, *122*, 9686–9689.

[4] S. W. Chen, R. S. Ingram, M. J. Hostetler, J. J. Pietron, R. W. Murray, T. G. Schaaff, J. T. Khoury, M. M. Alvarez, R. L. Whetten, *Science* **1998**, *280*, 2098–2101.

[5] a) S. Link, A. Beeby, S. FitzGerald, M. A. El-Sayed, T. G. Schaaff, R. L. Whetten, *J. Phys. Chem. B* **2002**, *106*, 3410–3415; b) M. A. El-Sayed, *Acc. Chem. Res.* **2001**, *34*, 257–264; c) S. Empedocles, M. Bawendi, *Acc. Chem. Res.* **1999**, *32*, 389–396.

[6] a) W. Chen, N. B. Zuckerman, X. W. Kang, D. Ghosh, J. P. Konopelski, S. W. Chen, *J. Phys. Chem. C* **2010**, *114*, 18146–

18152; b) K. Liu, X. W. Kang, Z. Y. Zhou, Y. Song, L. J. Lee, D. Tian, S. W. Chen, *J. Electroanal. Chem.* **2013**, *688*, 143 – 150.
[7] P. A. Bartlett, B. Bauer, S. J. Singer, *J. Am. Chem. Soc.* **1978**, *100*, 5085 – 5089.
[8] W. Chen, S. W. Chen, *Angew. Chem. Int. Ed.* **2009**, *48*, 4386 – 4389; *Angew. Chem.* **2009**, *121*, 4450 – 4453.
[9] M. J. Hostetler, J. E. Wingate, C. J. Zhong, J. E. Harris, R. W. Vachet, M. R. Clark, J. D. Londono, S. J. Green, J. J. Stokes, G. D. Wignall, G. L. Glish, M. D. Porter, N. D. Evans, R. W. Murray, *Langmuir* **1998**, *14*, 17 – 30.
[10] Y. Y. Yang, S. W. Chen, *Nano Lett.* **2003**, *3*, 75 – 79.
[11] a) Y. S. Sohn, D. N. Hendrick, H. B. Gray, *J. Am. Chem. Soc.* **1971**, *93*, 3603 – 3612; b) Y. S. Sohn, D. N. Hendrickson, J. H. Smith, H. B. Gray, *Chem. Phys. Lett.* **1970**, *6*, 499 – 501.
[12] a) X. Yuan, Z. T. Luo, Q. B. Zhang, X. H. Zhang, Y. G. Zheng, J. Y. Lee, J. P. Xie, *ACS Nano* **2011**, *5*, 8800 – 8808; b) T. Laaksonen, V. Ruiz, P. Liljeroth, B. M. Quinn, *Chem. Soc. Rev.* **2008**, *37*, 1836 – 1846; c) J. Akola, M. Walter, R. L. Whetten, H. Hakkinen, H. Gronbeck, *J. Am. Chem. Soc.* **2008**, *130*, 3756 – 3757.
[13] X. W. Kang, S. W. Chen, *Nanoscale* **2012**, *4*, 4183 – 4189.
[14] M. B. Robin, P. Day, *Adv. Inorg. Chem. Radiochem.* **1968**, *10*, 247 – 422.
[15] F. Z. Ding, H. B. Wang, Q. Wu, T. Van Voorhis, S. W. Chen, J. P. Konopelski, *J. Phys. Chem. A* **2010**, *114*, 6039 – 6046.
[16] S. Pradhan, S. W. Chen, S. Z. Wang, J. Zou, S. M. Kauzlarich, A. Y. Louie, *Langmuir* **2006**, *22*, 787 – 793.
[17] a) M. Conte, H. Miyamura, S. Kobayashi, V. Chechik, *J. Am. Chem. Soc.* **2009**, *131*, 7189 – 7196; b) R. Sharma, G. P. Holland, V. C. Solomon, H. Zimmermann, S. Schiffenhaus, S. A. Amin, D. A. Buttry, J. L. Yarger, *J. Phys. Chem. C* **2009**, *113*, 16387 – 16393; c) Y. Yu, Z. T. Luo, D. M. Chevrier, D. T. Leong, P. Zhang, D. E. Jiang, J. P. Xie, *J. Am. Chem. Soc.* **2014**, *136*, 1246 – 1249.
[18] a) W. Chen, J. R. Davies, D. Ghosh, M. C. Tong, J. P. Konopelski, S. W. Chen, *Chem. Mater.* **2006**, *18*, 5253 – 5259; b) W. Chen, N. B. Zuckerman, J. W. Lewis, J. P. Konopelski, S. W. Chen, *J. Phys. Chem. C* **2009**, *113*, 16988 – 16995; c) W. Chen, N. B. Zuckerman, J. P. Konopelski, S. W. Chen, *Anal. Chem.* **2010**, *82*, 461 – 465.

Received: September 25, 2015
Revised: November 9, 2015
Published online: December 8, 2015

